Check for updates

Quantitative turbidimetric characterization of stabilized complex coacervate dispersions†

Advait Holkar, [a] Shang Gao, [a] Kathleen Villaseñor, [a] Michael Lake[bc] and Samanvaya Srivastava ⭐[abcd]

Stabilizing complex coacervate microdroplets is desirable due to their various applications, such as bioreactors, drug delivery vehicles, and encapsulants. Here, we present quantitative characterization of complex coacervate dispersion stability inferred by turbidimetry measurements. The stability of the dispersions is shown to be modulated by the concentrations of comb polyelectrolyte (cPE) stabilizers and salt. We demonstrate cPEs as effective stabilizers for complex coacervate dispersions independent of the chemistry or length of the constituent polyelectrolytes, salts, or preparation routes. By monitoring the temporal evolution of dispersion turbidity, we show that cPEs suppress microdroplet coalescence with minimal change in microdroplet sizes over 48 hours, even at salt concentrations up to 300 mM. The number density and average microdroplet size are shown to be controlled by varying the cPE and salt concentrations. Lastly, turbidity maps, akin to binodal phase maps, depict an expansion of the turbid two-phase region and an increase in the salt resistance of the coacervates upon the introduction of cPEs. The coacervate salt resistance is shown to increase by $>3\times$, and this increase is maintained for up to 15 days, demonstrating that cPEs impart higher salt resistance over extended durations.

Introduction

Complex coacervates have garnered significant attention, emerging as attractive protocell candidates suitable for investigating fundamental biological systems[1,2] and as scalable synthetic bioreactors.[3] They form by associative liquid–liquid phase separation of oppositely charged macromolecules,[1,4–8] possess a distinct membraneless water–water interface with the ambient aqueous environments,[5,9,10] and have a strong propensity to partition and encapsulate charge-bearing macromolecules, including proteins[11–16] and nucleic acids.[17–21] The interior of the coacervate microdroplets comprises a crowded environment, which has been shown to affect polypeptide secondary structures[22–24] and protein folding,[14,25–27] improve enzyme activity,[26,28–31] and enhance DNA transcription rates.[17] Complex coacervate microdroplets can, therefore, provide a significantly simplified alternative to the natural cellular

chassis while still maintaining its critical features, including compartmentalization,[11,15,16,32,33] stimuli responsiveness,[11,14,34,35] selective molecular uptake,[34,36] biomacromolecular sequestration,[11–14,16] chemical conversions,[3,18,19,30,31,37] and macromolecular crowding.[14,23,27] Owing to the non-specificity and ubiquity of Coulombic interactions in myriad environmental conditions, these charge-driven self-assemblies have also been proposed as protocells in origin-of-life scenarios.[38,39] Moreover, complex coacervate microdroplets can also be used for drug delivery,[35,40,41] wastewater treatment,[42–44] as pesticide encapsulants,[45,46] and in cosmetic products.[47–49]

Stabilization of the liquid–liquid coacervate–water interface, however, is necessary to mitigate their macrophase separation and realize these applications at scale.[50] Prior approaches to stabilize coacervate microdroplets have employed lipids,[2,33,51] polymersomes,[32,33] colloidsomes,[52,53] proteinosomes,[53–55] novel polymers,[3,13,56] and microfluidic methods.[30,57–60] These approaches predominantly rely on the introduction of a hydrophobic layer around the microdroplets, in effect transforming the coacervate–water interface into juxtaposed coacervate–oil and oil–water interfaces, thus hindering molecular transport, resulting in long-term microdroplet instability, and suffering from a lack of scalability from the use of specialty materials.[3,50] In a significant departure from these approaches, our recent work demonstrated long-term stability (>4 months) of complex coacervate microdroplets using hydrophilic comb polyelectrolyte (cPEs) stabilizers.[3] Mixtures of oppositely charged

a Chemical and Biomolecular Engineering, University of California, Los Angeles, Los Angeles, CA 90095, USA. E-mail: samsri@ucla.edu

b NSF BioPACIFIC MIP, University of California, Los Angeles, Los Angeles, CA 90095, USA

c California NanoSystems Institute, University of California, Los Angeles, Los Angeles, CA 90095, USA

d Institute for Carbon Management, University of California, Los Angeles, Los Angeles, CA 90095, USA

† Electronic supplementary information (ESI) available. See DOI: **https://doi.org/10.1039/d3sm01761c**

homopolyelectrolytes and cPEs stabilizers self-assemble spontaneously, resulting in stable complex coacervate microdroplets. Moreover, the cPE stabilizers did not impede protein partitioning into the coacervate microdroplets and enabled bioreactions with significantly higher and tunable reaction rates.[3]

Given the diversity of charged macromolecules, complex coacervates with a tremendous range of physicochemical identities and properties are available for technological innovations.[61–63] Coacervates with different polymer lengths and architectures,[64–66] salt identities,[67] solution composition,[68] and environmental conditions[69,70] have been investigated, enabling prediction and control over properties such as their compositions and phase behavior,[68] density,[71,72] surface tension,[5,9,10] and rheology.[73,74] To effectively harness this diversity towards droplet-based applications, a universal and robust interfacial stabilization strategy is necessary. In this work, we present a comprehensive investigation towards understanding and quantifying the stabilization of coacervate microdroplets by cPEs. We demonstrate the cPE-driven stabilization of coacervate microdroplets, composed of weak or strong polyelectrolytes, with varying chain lengths. We also demonstrate the mixing protocol-independent stabilization of the coacervate microdroplets. Moreover, the temporal stability of the coacervate microdroplets is quantified to highlight the cPE-induced near-complete suppression of microdroplet coalescence, even in the presence of salt. In doing so, we also present a quantitative methodology for turbidimetric evaluation of coacervate dispersions. By constructing turbidity maps akin to binodal phase maps of coacervation, we demonstrate a $>3\times$ increase in the salt resistance of the coacervate phase in cPE-stabilized dispersions. The use of cPEs, therefore, provides a general and facile approach for stabilizing the coacervate–water interface and enabling their utility in diverse applications.

Materials and methods

Materials

Poly(acrylic acid sodium salt) of different molecular weights (M_W) (PAA, M_W = 3000, 5100, 15 000 g mol^{-1} with chain lengths (n) of 31, 53, and 160, respectively), polystyrene sulfonate (PSS, M_W = 70 000 g mol^{-1}, n = 340), sodium chloride (NaCl), and potassium bromide (KBr) were obtained from Millipore Sigma. PAA (M_W = 60 000 g mol^{-1}, n = 638) and poly(diallydimethylammonium chloride) (PDADMA, M_W = 8500 g mol^{-1}, n = 54) were obtained from Polysciences Inc. Comb polyelectrolyte polymethacrylic acid-*comb*-polyethylene glycol (PmAA$_{45}$-*comb*-PEG$_{68}$, 12 PEG side chains per comb-polyelectrolyte chain, 26 e$^-$ eq. per mol at pH = 6, polydispersity index 1.85) was provided by Master Builders Construction Chemicals.

Preparation of coacervate dispersions

Polyelectrolytes (PEs), cPE, and salt stock solutions were prepared in deionized water at appropriate concentrations. 5 mL of complex coacervate dispersions were prepared in scintillation vials and microcentrifuge tubes by mixing the oppositely charged PEs (PAA-PDADMA or PSS–PDADMA), cPE, and salt in the following order: mix water, salt, and polycation solution, vortex for 5 s, add cPE solution, vortex for 5 s, add polyanion solution, and vortex for 5 s.[6] This order of mixing was followed for all dispersions, except those prepared in the resuspension studies. For the resuspension studies, a 2 mL volume of sample was prepared in the following order: mix water, polycation solution, and polyanion solution, vortex for 5 s, centrifuge for 10 min at 500 × g, add cPE solution, and vortex for 5 s. NaCl was used to test the salt resilience of the PAA-PDADMA coacervate microdroplets, and KBr (1.8 M) was used in preparing the PSS–PDADMA coacervate microdroplet dispersions.

In all the dispersions, unless noted otherwise, the oppositely charged PEs were added in *homopolyelectrolyte-charge-matched* concentrations, and the cPE contributed to additional macromolecular charge. In the *overall-charge-matched* dispersions (discussed in Fig. 2A), the positive charge from the polycation and the combined negative charge from the polyanion and the anionic cPE were matched.

High throughput preparation of coacervate dispersions

The Fluent Automated Workstation by Tecan was used for the preparation of coacervate dispersions in transparent flat-bottom 96 well plates. 200 μL of coacervate dispersions were prepared by mixing the appropriate volumes of PEs, cPE, and salt stock solutions. The order of mixing was water, polycation, comb-polyelectrolyte, and polyanion. cPE was added by immersing the pipette tips into the solution in the well to avoid bubble formation. To mix the components, 50 μL volume was aspirated and dispersed 3 times following each mixing step.

Absorbance measurements

Single wavelength and kinetic, multiwavelength absorbance measurements were conducted on the Tecan Spark multimode microplate reader. For the single wavelength measurements, absorbance at 400 nm was measured at 9 spots in each well after orbital shaking of the plate for 5 seconds at 2 mm amplitude in the Tecan Spark microplate reader. Absorbance measurements were carried out on *as mixed* dispersions (within 2 minutes of their preparation) and after 24 hours, 48 hours, and 15 days. The orbital mixing step was carried out before each measurement. Plates were sealed after the absorbance measurements by the Thermo Fischer ALPS5000 Automated Plate Heat Sealer at 170 °C and stored at room temperature. The plates were resealed after every measurement.

The evolution of the microdroplet population density was ascertained by carrying out absorbance measurements at 400, 500, 600, 700, and 800 nm at 10-minute intervals for 3 hours at 1 spot in each well, starting within 2 minutes of sample preparation. The path length l for all measurements was 0.25 cm.

Dynamic light scattering

Dynamic light scattering (DLS) experiments were performed with the Malvern Zetasizer at a scattering angle of 173° with the zen0040 cuvette. The shearing of samples was minimized by

manually preparing dispersions in 96 well plates with a volume of 300 μL. The order of mixing was water, polycation, comb-polyelectrolyte, and polyanion. The dispersion was mixed by aspirating and dispersing 50 μL volume 3 times before conducting a measurement. Three measurements were conducted for every sample, and correlograms obtained were averaged and fitted by the cumulants method to obtain average sizes and polydispersity indices. A minimum derived count rate of 1000 kilo counts per second was maintained by conducting every measurement for 2 minutes. The correlogram obtained had minimal to no noise for all samples, and the correlogram for the three measurements did not deviate from each other significantly, indicating very little sedimentation during the measurements.

Optical microscopy

Brightfield microscopy was carried out to visualize the coacervate–water interface and detect changes in chemical equilibrium by cPE addition using a $63\times$ and $40\times$ objective lens. Solutions of PAA ($n = 53$) and PDADMA ($n = 54$) were prepared with $C_{PE} = 70$ mM and centrifuged to separate the supernatant from the settled coacervate phase. 10 μL of the coacervate phase was extracted, placed on a cover slip, and imaged under the microscope. Following this, 20 μL of the supernatant, cPE-supernatant, or PAA-supernatant were brought into contact with the coacervate microdroplets. Micrographs near the coacervate–supernatant interface were captured within 5 minutes of preparation.

Results

Robust stabilization of complex coacervate microdroplets by comb polyelectrolytes

We established the robustness of stabilization of complex coacervate dispersions by showing improved microdroplet stability against coalescence in the presence of different salts and distinct polymer chemistries (Fig. 1). These results provide further credence to our previous work, wherein the addition of comb polyelectrolytes (cPEs) was shown to stabilize complex coacervate dispersions (Fig. 1A) for up to 48 hours.[3] Furthermore, while microdroplets settled over 4 months, they did not coalesce and macrophase separate.[3] The charged backbone of the cPEs is posited to allow cPE chains to localize on coacervate microdroplet surfaces, and the hydrophilic side chains reduce microdroplet coalescence by providing steric repulsion while allowing the transfer of small molecules owing to the lack of a membrane.

Even in the presence of salt, cPEs stabilized coacervate dispersions. Electrostatic screening by the salt ions weakens the interactions among the oppositely charged polyelectrolytes (PEs) and their propensity to form complexes; and can also interfere with the stabilization of the coacervate microdroplets by cPEs. Fig. 1B shows PE-charge-matched complex coacervate dispersions prepared with PAA$_{54}$ and PDADMA$_{53}$ with $C_{PE} = 62.2$ mM, $C_{cPE} = 4.8$ mM, and $C_{NaCl} = 0.2$ M. Here, C_{PE} and

C_{cPE} indicate the concentrations of the ionic moieties contributed by the PE and cPE chains, respectively, and C_{NaCl} indicates NaCl concentration in the coacervate dispersions. The prepared mixtures were turbid, indicating a two-phase mixture. The presence of coacervate microdroplets was confirmed by microscopy. After 48 hours, a gradient in turbidity with higher turbidity towards the bottom of the vial was observed, indicating partial settling. The corresponding micrograph showed the presence of coacervate microdroplets, qualitatively demonstrating that cPEs stabilize coacervate microdroplets even in the presence of salt. In contrast, in the absence of cPE, macrophase separation occurred within 3 hours, even at low NaCl concentrations of 0.05 M (Fig. S1, ESI†).

cPEs also effectively stabilized coacervate dispersions comprising strong polyelectrolytes. To emphasize the versatility of cPEs as stabilizers, coacervate dispersions with a strong polyanion PSS$_{340}$, PDADMA$_{53}$, and KBr ($C_{PE} = 116.4$ mM, $C_{cPE} = 50$ mM, $C_{KBr} = 1.8$ M) were prepared. PSS–PDADMA mixtures form solid-like precipitates instead of liquid-like coacervates in the absence of added salt.[71,72] Salt is typically added to screen electrostatic interactions and plasticize the complexes to yield liquid-like coacervates.[71,72] KBr was used as it screens electrostatic interactions more effectively than NaCl[72,75] to yield liquid PSS–PDADMA coacervates. As evident in Fig. 1C, turbidity and microdroplets were observed both *as mixed* dispersions and after 48 hours. While a decrease in turbidity over 48 hours of sample preparation was noted at low C_{cPE}, turbidity persisted beyond $C_{cPE} > 30$ mM up to 48 hours (Fig. S2, ESI†). We note that higher C_{cPE} was required for the long-term stability of the PSS–PDADMA dispersions as compared to PAA-PDADMA dispersions. The strong electrostatic screening at high KBr concentration is posited to weaken the interaction of cPE with the microdroplet surface, potentially requiring a higher C_{cPE} for a similar extent of chain localization on microdroplet surfaces.

The PE length had little influence on the stability of the coacervate dispersions. The influence of PE length on dispersion stabilization was investigated with complex coacervates comprising PDADMA$_{53}$ and PAA of different chain lengths ($n = 32$, 160, and 638). Dispersions with $C_{PE} = 38.8$ mM and $C_{cPE} = 4.8$ mM were prepared in the absence of salt (Fig. 1D). The turbidity of the dispersions persisted for 48 hours, demonstrating that complex coacervate microdroplets composed of PEs with asymmetric chain lengths can also be stabilized by cPE addition.

Microdroplet stabilization is hypothesized to emerge from steric repulsion between the neutral cPE sidechains, with minimal contributions from the excess surface charges due to cPE localization on microdroplet surfaces. To minimize the influence of electrostatic repulsion on microdroplet stabilization, we investigated dispersions wherein the positive charge from the polycation and the combined negative charge from the polyanion and the anionic cPE were matched. The cPE-containing *overall-charge-matched* PAA$_{53}$-PDADMA$_{54}$ dispersions ($C_{PE} = 70$ mM) remained turbid until 48 hours after preparation, with no apparent settling at high C_{cPE} (Fig. 2A), again indicating suitable stabilization of the dispersions.
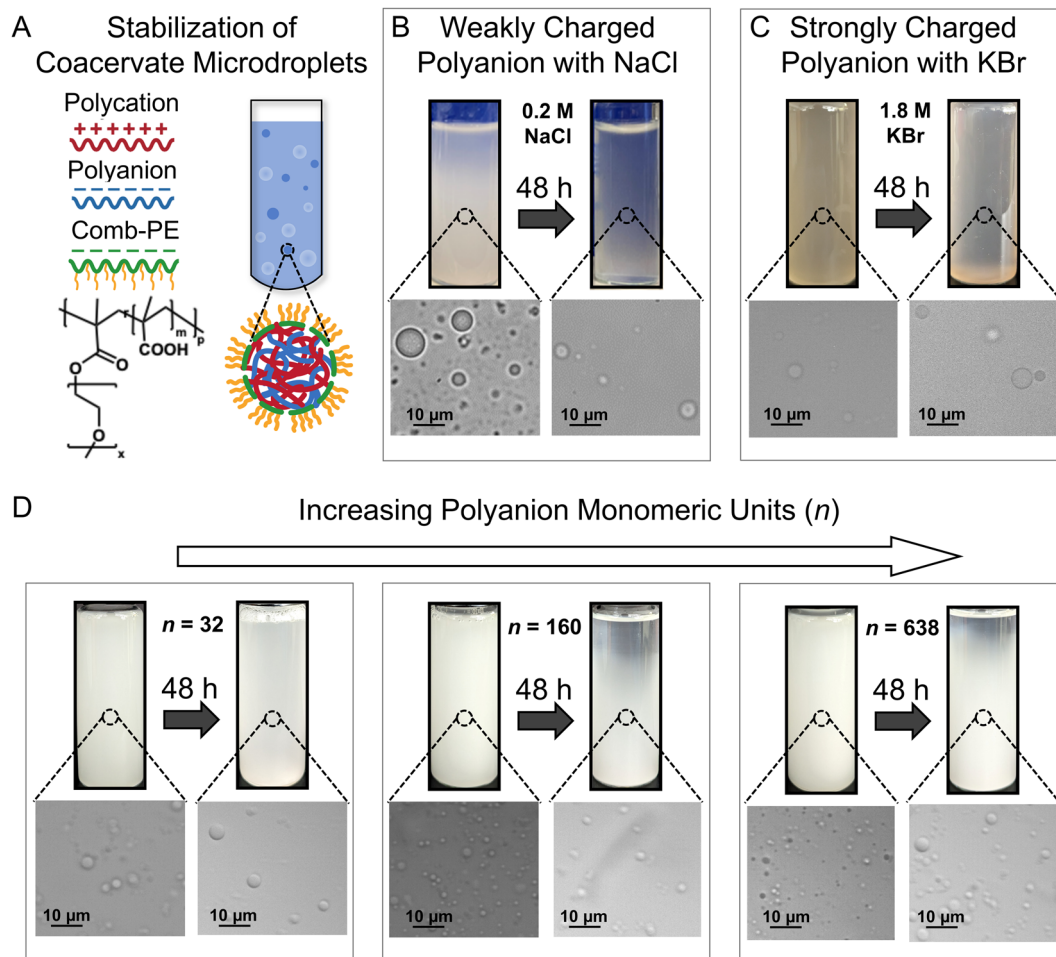
Fig. 1 Comb polyelectrolytes (cPEs) stabilize complex coacervate microdroplets. (A) Mixing of oppositely charged polyelectrolytes (1 : 1 charge ratio) in the presence of cPEs stabilizes the complex coacervate microdroplets against coalescence, resulting in turbid dispersions. r refers to the random copolymer cPEs comprising methacrylic acid and PEG methacrylate. The average values of m, x, and p for the cPEs used in this study are 3.7, 68, and 12.1, respectively. (B) Complex coacervate microdroplets formed with PDADMA (degree of polymerization $n = 53$) and PAA ($n = 54$), a weak polyelectrolyte, with 0.2 M NaCl were stabilized by anionic cPE. Here, $C_{PE} = 62.2$ mM and $C_{cPE} = 4.8$ mM. (C) Droplets formed with PDADMA ($n = 53$) and PSS ($n = 340$), a strong polyelectrolyte, with 1.8 M KBr were also stabilized by anionic cPE. Here, $C_{PE} = 116.4$ mM and $C_{cPE} = 50$ mM. (D) Coacervate microdroplets with PDADMA ($n = 53$) and PAA (varying n) were stabilized by cPE, indicating that cPEs can stabilize complexes with asymmetric linear PEs. In (B)–(D), dispersion turbidity persisted for 48 hours, and coacervate microdroplets were noted in the corresponding micrographs.

The stabilization of the dispersions was established to be resilient to the order of polymer mixing and microdroplet formation routes. Our previous work established that microdroplet stabilization was independent of the mixing order of the PEs and cPEs.[3] We further probed the robustness of the stabilization mechanism by conducting concomitant redispersion and stabilization of coacervate phases, depicted schematically in Fig. 2B. Coacervates were prepared by mixing the oppositely charged PEs (without cPE addition) and centrifuged to separate the coacervate and the supernatant phases. cPE, at varying concentrations, was subsequently introduced in the supernatant, followed by vigorous vortex mixing to resuspend the coacervate as microdroplets, yielding turbid dispersions (Fig. 2C). In contrast to the resuspended *as vortexed* dispersions with no cPE that became clear again within a few hours owing to the macrophase separation of the coacervate and supernatant phases, the turbidity of the dispersions containing cPEs persisted over 48 hours (Fig. 2C), indicating that cPEs stabilized the resuspended coacervate microdroplet. While partial settling was observed in dispersions with low C_{cPE} (≤ 4 mM), no settling was visually apparent at higher C_{cPE} (≥ 6 mM), indicating that higher C_{cPE} improve dispersion stability.

Temporal evolution of stabilized coacervate dispersions

The average microdroplet size of the stabilized dispersions is tunable *via* variation of C_{PE}, C_{cPE}, and C_{salt}. Our previous work demonstrated the interplay between C_{PE} and C_{cPE} in dictating microdroplet size.[3] Here, we investigate the variation of microdroplet sizes in PAA$_{54}$–PDADMA$_{53}$ ($C_{PE} = 70$ mM) with varying C_{cPE} and C_{NaCl} using dynamic light scattering (DLS). We denote the turbidity, the average microdroplet diameter, and number density as T, d, and N, respectively, and their initial values obtained for *as mixed* dispersions are denoted by T_0, d_0, and N_0, respectively.
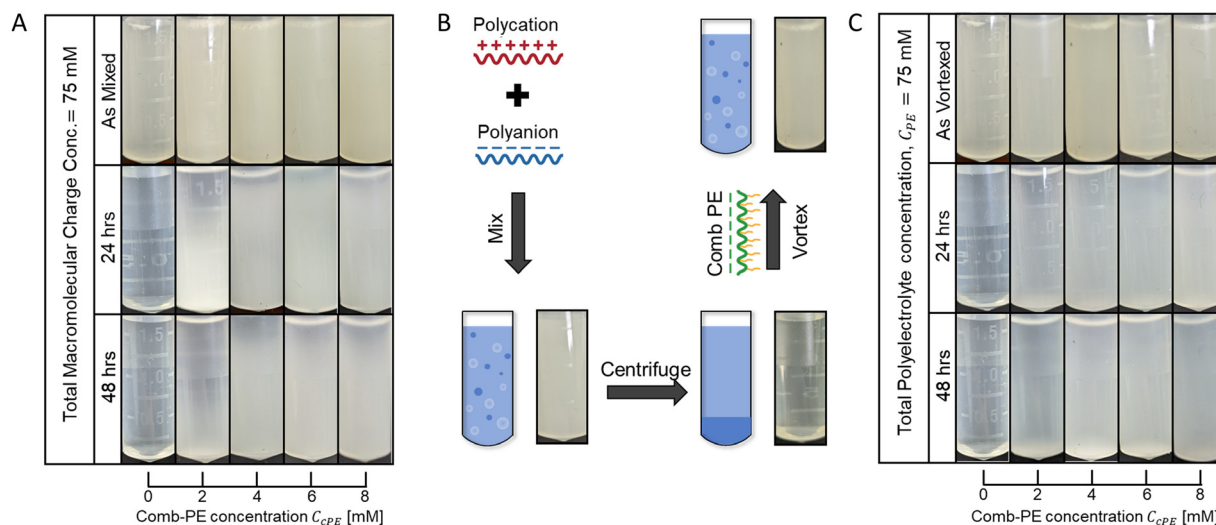
Fig. 2 cPEs provide robust stabilization to complex coacervate microdroplets. (A) Complex coacervate microdroplets in a mixture with a 1:1 ratio of positive macromolecular charge to negative macromolecular charge from both polyanion and anionic comb-polyelectrolyte are stable against coalescence for up to 48 hours. Photographs show *as mixed* dispersions and dispersions after 24 and 48 hours. Increasing C_{cPE} improved dispersion stability. (B) and (C) Resuspension of complex coacervate macrophase in the presence of cPEs yields stable dispersions. (B) Schematics depicting the redispersion procedure. (C) Photographs show *as vortexed* dispersions and dispersions after 24 and 48 hours. Again, increasing C_{cPE} improved dispersion stability.

For *as mixed* dispersions, d_0 decreased with increasing C_{cPE} and increased with increasing C_{NaCl} (Fig. 3A). Moreover, the relative reduction in d_0 with increasing C_{cPE} diminished with increasing C_{NaCl}. We hypothesize that the droplet sizes are dictated by the ratio of the coacervate phase volume (dictated by C_{PE} and C_{NaCl}) and the interfacial area that can be stabilized (dictated by C_{cPE}). As C_{cPE} increases, a larger interfacial area can be stabilized by the cPE chains, while the coacervate phase volume remains the same, resulting in more, smaller microdroplets in the dispersions and a smaller d_0. Conversely, with increasing C_{NaCl}, the volume of the coacervate phase increases (higher water content in the coacervate phase) while the interfacial area that can be stabilized in the dispersions remains similar (owing to constant C_{cPE}), leading to larger d_0. A plateau in d_0 with increasing C_{cPE} is also observed, indicating that microdroplet size may not continually decrease with excess cPE addition, perhaps owing to the formation of cPE bilayers and vesicular structures.

The size distribution estimated from DLS measurements (Fig. 3A) was coupled with turbidimetric measurements to estimate N_0 in *as mixed* dispersions. Absorbance measurements have been employed extensively, albeit qualitatively, to detect complexation.[76,77] Here, we employ quantitative analysis of the absorbance measurements to obtain dispersion characteristics. The absorbance A of the dispersions was measured, and the T was calculated as:

$$T = \ln(10) \times A/l \tag{1}$$

where l is the path length of the sample. The turbidity T of the dispersions decreased with increasing C_{NaCl} (Fig. 3B), which was expected since salt screens electrostatic interactions between the charged polymers and hinders coacervation.

At the same time, an increase in T was noted with increasing C_{cPE} indicating an increase in the number density of the microdroplets in the dispersions. With the assumption of single scattering events, T is related to microdroplet diameter d and number density N for a monodisperse dispersion as:[78]

$$T \sim Nd^2Q(d, \lambda) \tag{2}$$

where Q is the scattering coefficient dependent on d and wavelength λ. Since d is comparable to λ, Q is calculated by the general Mie Theory (Fig. S3, ESI†).[78,79] For a polydisperse system, eqn (2) is modified as:

$$T \sim N\int_0^\infty a^2f(a)Q(a, \lambda)\mathrm{d}a \tag{3}$$

where f is the population distribution function. Thus, with f estimated from DLS measurements (Fig. 3A) and T_0 estimated from absorbance measurements (Fig. 3B), microdroplet number density N_0 was estimated as a function of C_{cPE} and C_{NaCl} (Fig. 3C).

Increasing C_{cPE} increased N_0, and increasing C_{NaCl} decreased N_0 (Fig. 3C). Moreover, a plateau in N_0 with increasing C_{cPE} was observed, similar to that observed for d_0. Thus, we posit an optimum C_{cPE} for a given C_{NaCl} and C_{PE}, beyond which the addition of cPEs does not decrease the microdroplet size or increase their number density, indicating a saturation of the interfacial area stabilized by the cPE chains.

The temporal evolution of the turbidity of the dispersions enabled quantification of the stability of coacervate microdroplets (Fig. 4A–C). The turbidity was expected to decrease with time due to the coarsening of the dispersions and sedimentation of the microdroplets. In the unstable dispersions (without any cPE stabilizers), a rapid decrease in turbidity was observed;
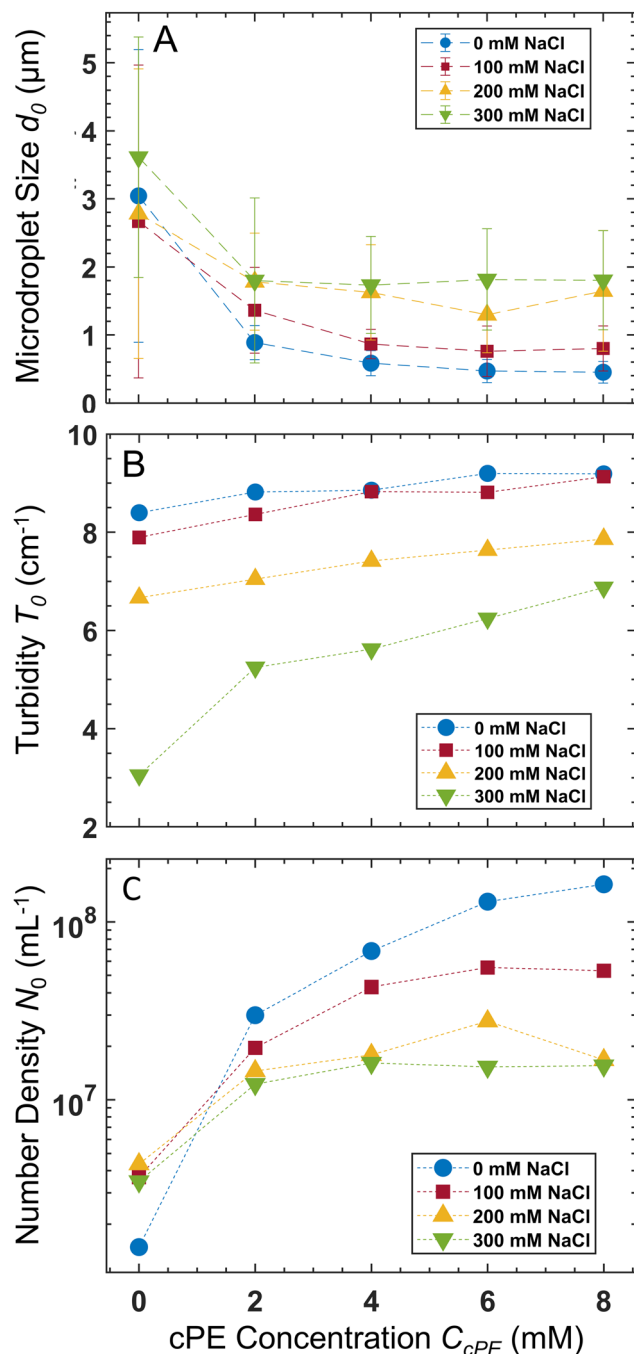
Fig. 3 Complex coacervate microdroplet size and number density can be tuned by comb-polyelectrolyte concentration. (A) The initial average microdroplet size decreases with C_{cPE} and increases with C_{salt}. (B) In contrast, the initial turbidity of the dispersion (measured at 400 nm) increases with C_{cPE} and decreases with C_{salt}. (C) The microdroplet number density, estimated from the microdroplet size and dispersion turbidity, mimics turbidity trends.

the turbidity vanished within 3 hours. In contrast, turbidity decay in cPE-stabilized dispersions ($C_{cPE} = 4$ mM and 8 mM) was significantly slower; substantial turbidity remained after 3 hours, even at the highest salt concentration studied. The evolution of the microdroplet population was estimated from

the temporal evolution of the microdroplet number density, $N(t)$, by approximating the scattering coefficient $Q(d, \lambda)$ as:[80]

$$Q(d,\lambda) = Q_0(d/\lambda)^m \qquad (4)$$

where Q_0 is a constant and m is dependent on d and λ. Combining eqn (3) and (4) yields:

$$T(\lambda) = \text{constant} \times (\lambda)^m \qquad (5)$$

m was obtained by measuring τ over a spectrum of wavelengths (Fig. S3, ESI†). Then, following the procedure described by Reddy and Fogler,[80] normalized average microdroplet size as a function of time was estimated as:

$$\bar{d}(t) = \frac{d(t)}{d_0} \sim \left[\left(\frac{T(t)}{T_0} \right) \left(\frac{d_0}{\lambda} \right)^{m_0 - m(t)} \right]^{\frac{1}{m-1}} \qquad (6)$$

where d_0, m_0, and T_0 are the initial values for the average microdroplet size, exponent, and turbidity, respectively. $m(t)$ was calculated from absorbance measurements of τ at different λ performed over 3 hours (Fig. S4, ESI†).

In the absence of cPE, along with decreasing turbidity, average microdroplet size increases rapidly with an approximate power-law of $\bar{d}(t) \sim t^{0.8}$ at longer times. Furthermore, $\bar{d}(t)$ appeared independent of C_{NaCl}, indicating that the dominant coarsening mechanism is independent of C_{NaCl}. This is expected in the case of unrestricted coalescence, given the large microdroplet number densities N (Fig. 3C) and that rate of coalescence scales as $\sim N^2$.[81,82]

In contrast, no significant coarsening was observed in dispersions comprising cPEs, indicating that adding cPEs suppresses droplet coalescence. These results are also consistent with our previous observations of microdroplet persistence over months.[3] In dispersions with 8 mM cPE, $d/d_0 \sim 1$ in no added salt dispersions and $d/d_0 \sim 1.1$ in dispersions with 300 mM salt, up to 3 hours. To support these findings, microdroplet size evolution was also observed over 48 hours with varying salt concentrations using DLS (Fig. S5, ESI†), and the microdroplet size was found to remain nearly constant in the cPE-stabilized dispersions. Hence, we can surmise that the stability of the coacervate microdroplets can be significantly improved, even at high salt concentrations, by adding cPEs.

Turbidity maps of stabilized coacervate dispersions

Turbidity of the coacervate dispersions (Fig. S6–S9, ESI†) decreased with increasing C_{NaCl} until they became transparent. Upon progressive introduction of cPEs, the dispersions became more turbid, and the turbidity persisted up to higher C_{NaCl}. From these measurements, turbidity gradients were calculated to construct contour lines with constant turbidity in the C_{PE}–C_{NaCl} plane at constant C_{cPE} and lower limits of 4, 6 and 8 cm^{-1} were assigned to obtain different regions of turbidity. The inverted-U shape of the turbid regions observed in Fig. 5A is akin to the two-phase region in binodal phase maps of polyelectrolyte complexes.[6,68,83–85]

For all C_{cPE}, turbidity decreased with increasing C_{NaCl} at a constant C_{PE}. Increasing C_{NaCl} reduces the coacervate
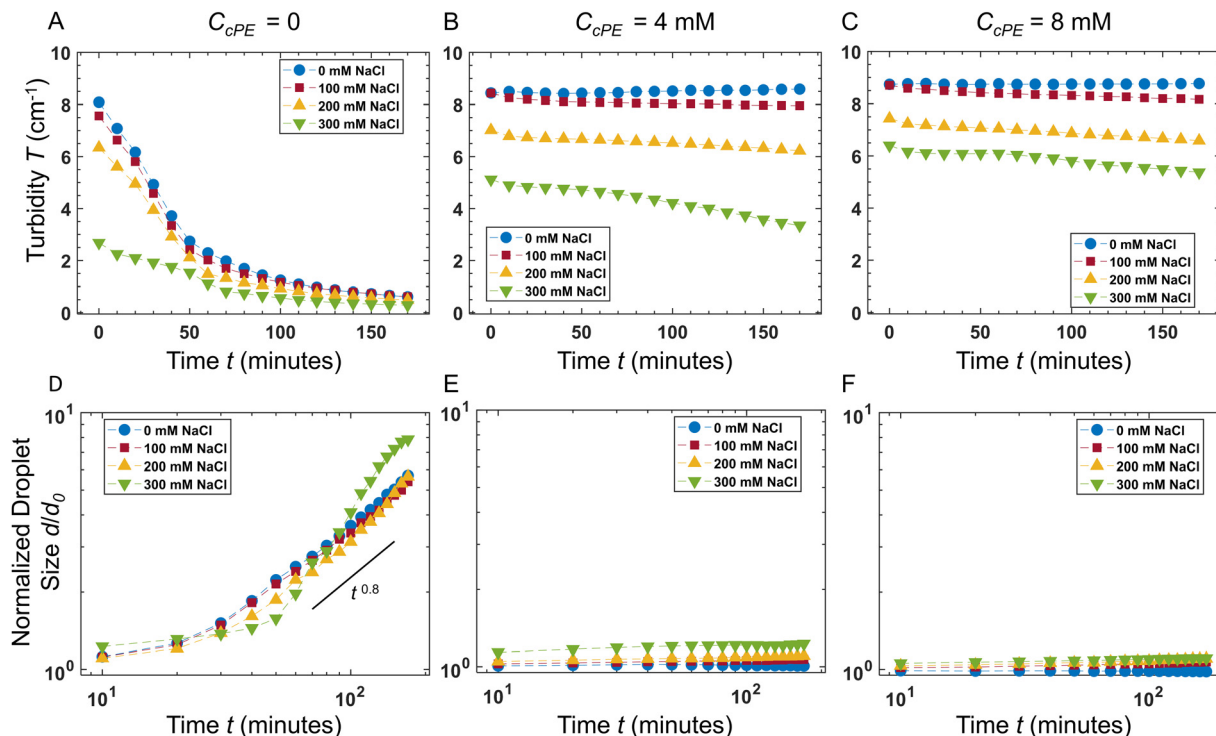
Fig. 4 Comb polyelectrolytes improve the stability of complex coacervate dispersions even in the presence of salt. The temporal evolution of (A)–(C) dispersion turbidity evaluated using a 500 nm incident light and (D)–(F) the normalized microdroplet size d/d_0 are shown for different salt and cPE concentrations. The rate of coarsening is significantly reduced by increasing cPE concentration, and stable droplets can be obtained even at salt concentrations up to 300 mM.

microdroplet number density N, lowering the turbidity of the dispersion. Also, within the two-phase window, turbidity evolved non-monotonically with C_{PE}, with higher turbidity at the center of the two-phase window. Increasing C_{PE} increases the volume of the coacervate phase available to be dispersed in the supernatant, responsible for the initial increase in turbidity with increasing C_{PE}. However, the increase in the coacervate volume fraction also increases the rate of coalescence of the microdroplets, forming larger microdroplets and reducing N at even higher C_{PE}, thereby reducing the turbidity.

Increasing C_{cPE} expanded the turbid two-phase regions for the *as mixed* samples with turbid solutions persisting at higher C_{NaCl}, since higher C_{cPE} increases N and increases microdroplet stability (Fig. 5A). Similarly, regions of high turbidity were observed in the center of the 2-phase region on increasing $C_{cPE} \geq 6$ mM due to smaller d and an increase in N. We also observed that the expansion of the two-phase window to higher salt concentrations was more pronounced at lower C_{cPE}. For a constant C_{cPE}, increasing C_{PE} decreases C_{cPE}/C_{PE}, leading to a lower availability of cPE chains and therefore reducing the stability at higher salt. This reduced turbidity can be, therefore, attributed to the formation of larger microdroplets and faster settling. We previously reported similar observations with improved temporal dispersion stability in the absence of salt at higher C_{cPE}/C_{PE}.[3] At the same time, in contrast to expansion to higher salt, expansion of the two-phase window along the PE concentration range was markedly

lower, indicating that the two-phase region is bound within the same PE concentrations as those found in the absence of cPEs.

We define salt resistance C_{NaCl}^* as the maximum salt concentration beyond which regions of no significant turbidity for a given C_{cPE} are observed, irrespective of C_{PE} (marked by dotted lines in Fig. 5). C_{NaCl}^* in *as mixed* systems increased nearly linearly from ~ 150 mM in the unstable dispersions ($C_{cPE} = 0$) to ~ 520 mM for the stabilized dispersions (with $C_{cPE} = 8$ mM). We note that $C_{cPE} = 8$ mM is still approximately 5-fold less than the C_{PE} of ~ 40 mM for which significant turbidity is still present at C_{NaCl}^*. Thus, we infer that coacervate microdroplets can persist at $\sim 3.5 \times$ higher salt concentrations upon adding relatively small amounts of cPEs. We hypothesize that an improvement in salt resistance (and improved interfacial stability), as estimated from the turbidity measurements, emerges from a combination of kinetic impediments to droplet coalescence and a perturbation of the thermodynamic equilibrium upon introducing cPEs.

The turbidity maps were also constructed after 24 hours (Fig. 5B), 48 hours (Fig. S10, ESI†), and 15 days (Fig. 5C). Expectedly, no turbidity was observed for unstable dispersions, while turbidity persisted in the stabilized dispersions for up to 15 days. However, due to microdroplet coarsening and settling, the turbidity windows contracted over time. This contraction was more pronounced at lower C_{cPE} as well as at lower C_{cPE}/C_{PE}, ratios, which was expected due to their lower stability. Fig. 6
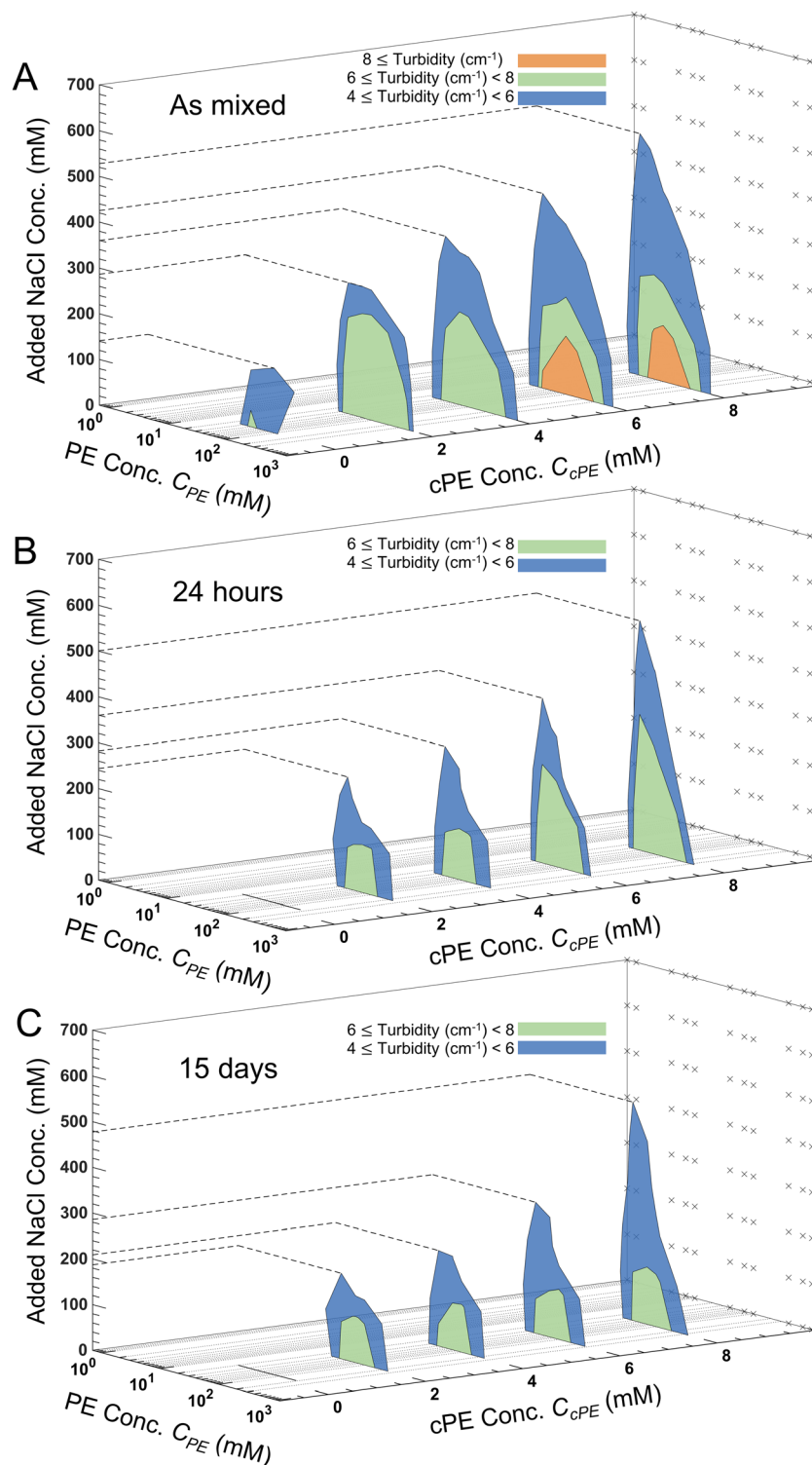
Fig. 5 Comb polyelectrolytes stabilize complex coacervate dispersions up to higher salt concentrations, expanding the window of turbidity. (A)–(C) Turbidity windows are shown over a range of polyelectrolyte (PE, 1:1 charge ratio) and salt concentrations at different comb polyelectrolyte (cPE) concentrations. Increasing cPE concentration is noted to expand the turbidity window, indicating the presence of stabilized microdroplets at higher salt concentrations. (A) shows the turbidity of the *as mixed* dispersions; (B) and (C) show turbidity windows of these dispersions after 24 hours and 15 days, respectively. The dotted lines denote the salt resistance of the dispersions corresponding to a constant C_{cPE}. The cross symbols on the back panel denote the C_{PE}–C_{NaCl} compositions where dispersion turbidity was measured.
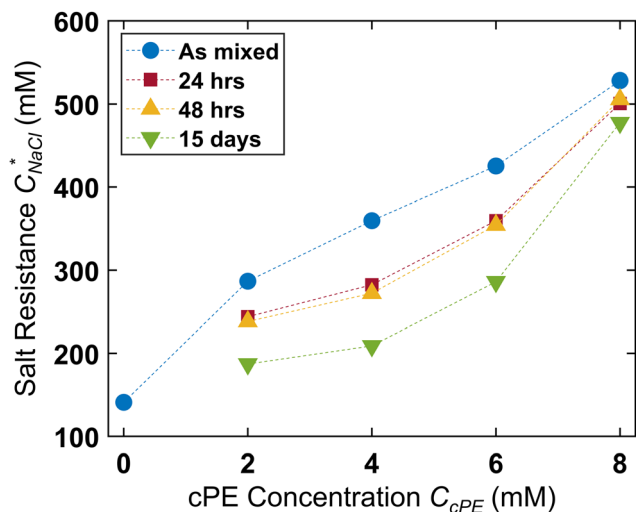
Fig. 6 The temporal evolution of the salt resistance C_{NaCl}^* for complex coacervate dispersions. C_{NaCl}^*, corresponding to the maximum salt concentration at which dispersions retained turbidity of 4 cm^{-1} irrespective of the PE concentration, is shown as a function of comb polyelectrolyte concentration. C_{NaCl}^* of the complex coacervate dispersions increases with increasing cPE concentration and is maintained for up to 15 days.

shows that C_{NaCl}^* decreased with time, and the largest decrease occurred within the first 24 hours; no significant changes occurred in the next 24 hours. As the dispersions continue to coarsen, C_{NaCl}^* lowered marginally after 15 days. This reduction in C_{NaCl}^* diminished at higher C_{cPE} due to the higher stability of the dispersions. For the highest C_{cPE} of 8 mM, $C_{NaCl}^* \sim 480$ mM was obtained even after 15 days, demonstrating that C_{cPE} addition can impart long-term stability to coacervate microdroplets even in the presence of salt.

Discussion and conclusions

Typical coacervate dispersions are unstable, and their kinetic stability is difficult to achieve and control.[86] Here, we have demonstrated a robust strategy for the long-term stabilization of complex coacervate microdroplets, which provides a platform to advance their technological potential as protocells,[1,2] bioreactors,[3] drug delivery vehicles,[35,40,41] and encapsulants.[45–49] On the addition of cPEs to the PE mixtures, the anionic backbone of the cPEs is expected to interact electrostatically with the polycations and have a strong tendency to assimilate within the coacervate microdroplets, while the neutral side chains are expected to prefer staying in the continuous phase. The latter is posited owing to the greater preference of the neutral chains to remain in less crowded spaces to maximize their entropy. This competition results in the pinning of the cPEs at the coacervate–water interface and provides steric hindrance against the coalescence of the microdroplets. We note that the stabilization of coacervate microdroplets is independent of the path taken to microdroplet generation (Fig. 2), further adding to our previous report[3] where we demonstrated stabilization independent of the

mixing order of the PEs and the cPE chains. Simultaneously, the microdroplet population is more stable in the presence of cPEs (Fig. 4), highlighting the robustness of the stabilized dispersions. While the average microdroplet size (d) in the absence of cPEs evolved with an approximate power law of $d \sim t^{0.8}$ at long times owing to unrestricted coalescence, it reduced to nearly time-independent d when coalescence was suppressed by cPE addition (Fig. 4). Coacervates with PE chain length asymmetry and *overall-charge-matched* systems are also stabilized (Fig. 1 and 2), demonstrating that cPEs can confer stability to a wide variety of coacervate dispersions.

Even in the presence of salt, the dispersions can be stabilized, albeit requiring higher C_{cPE} (Fig. 5 and 6). The addition of salt decreases the Debye length and weakens the Coulombic forces between charged macromolecules due to charge screening. Increasing C_{salt} not only inhibits the coacervation of the PEs but also reduces the electrostatic interaction of the negatively charged cPE backbone with the PEs in the coacervates. This screening reduces the extent of localization of the cPE chains, which, in turn, reduces the stability provided by its neutral side chains. Therefore, higher concentrations of cPEs are required to achieve stabilization. Furthermore, we show that d_0 can be tuned by changing the C_{NaCl} and C_{cPE}.

Turbidity maps with changing C_{cPE} were systematically constructed over a wide range of C_{PE} and C_{NaCl} spanning both the one-phase and the two-phase regions. Increasing C_{cPE} not only increased the turbidity within the 2-phase region but also at higher C_{NaCl} outside this region. The maximum salt concentration where significant turbidity is observed, C_{NaCl}^*, increases from ~ 150 mM in the absence of cPEs to ~ 520 mM at $C_{cPE} = 8$ mM. Even over 15 days, while dispersions with low C_{cPE} showed C_{NaCl}^* decrease to ~ 150 mM, dispersions with 8 mM cPE still showed a high C_{NaCl}^* of ~ 480 mM. Thus, we argue that cPE addition improved the salt resistance of coacervate microdroplets. To further probe the influence of cPEs on the equilibrium state of the coacervate phases, preliminary experiments were carried out where cPEs were added to macrophase-separated coacervates. A coacervate microdroplet, prepared with no added salt (PAA$_{54}$–PDADMA$_{53}$, $C_{PE} = 70$ mM) along with its supernatant was placed on a cover slip and observed under a microscope (Fig. S11A and B, ESI†). Subsequently, a small volume of concentrated cPE solution was introduced into the supernatant such that the overall C_{cPE} was 4 mM. A spontaneous emergence of microdroplets was observed near the interface on the supernatant solution side (Fig. S11C, ESI†), indicating that cPE addition perturbed the equilibrium between the coacervate and supernatant phases despite the relatively low added charge (4 mM cPE *vs.* 70 mM), as well as stabilized the perturbed state of the two-phase system. In contrast, introducing 4 mM excess PAA into the supernatant did not lead to any microdroplet formation (Fig. S11D, ESI†). These experiments provide sufficient evidence that cPEs influence the thermodynamics and interfacial composition of coacervates in non-trivial and intriguing ways and continue to motivate us to pursue future investigations in these directions.

Author contributions

The manuscript was written with contributions from all authors. All authors have given approval to the final version of the manuscript. Advait Holkar: conceptualization (equal), data curation (lead), formal analysis (lead), investigation (lead), methodology (lead), validation (lead), visualization (equal), writing – original draft (lead); Shang Gao: conceptualization (equal), investigation (supporting), methodology (supporting), writing – original draft (supporting); Kathleen Villasenor: investigation (supporting), methodology (supporting), writing – original draft (supporting); Michael Lake: investigation (supporting), methodology (supporting); Samanvaya Srivastava: conceptualization (equal), funding acquisition (lead), methodology (supporting), project administration (lead), resources (lead), supervision (lead), visualization (equal), writing – original draft (supporting), writing – review & editing (lead).

Conflicts of interest

The authors declare the following competing financial interest(s): A. H., S. G., and S. S. are inventors on Provisional Application #63/187,031, filed on 05/11/2021 and held by the University of California, Los Angeles, that covers the use of comb polyelectrolytes as stabilizers for complex coacervate microdroplets.

Acknowledgements

Notes and references

1 M. Abbas, W. P. Lipiński, J. Wang and E. Spruijt, *Chem. Soc. Rev.*, 2021, **50**, 3690–3705.

2 T. Y. Dora Tang, C. Rohaida Che Hak, A. J. Thompson, M. K. Kuimova, D. S. Williams, A. W. Perriman and S. Mann, *Nat. Chem.*, 2014, **6**, 527–533.

3 S. Gao and S. Srivastava, *ACS Macro Lett.*, 2022, **11**, 902–909.

4 I. K. Voets, A. de Keizer and M. A. Cohen Stuart, *Adv. Colloid Interface Sci.*, 2009, **147–148**, 300–318.

5 M. Iqbal, Y. Tao, S. Xie, Y. Zhu, D. Chen, X. Wang, L. Huang, D. Peng, A. Sattar, M. A. B. Shabbir, H. I. Hussain, S. Ahmed and Z. Yuan, *Biol. Proced. Online*, 2016, **18**, 1–18.

6 S. Srivastava and M. V. Tirrell, *Adv. Chem. Phys.*, 2016, **161**, 499–544.

7 B. Y. Zaslavsky, L. A. Ferreira and V. N. Uversky, *Biomolecules*, 2019, **9**, 473.

8 C. E. Sing and S. L. Perry, *Soft Matter*, 2020, **16**, 2885–2914.

9 E. Spruijt, J. Sprakel, M. A. Cohen Stuart and J. Van Der Gucht, *Soft Matter*, 2009, **6**, 172–178.

10 J. Qin, D. Priftis, R. Farina, S. L. Perry, L. Leon, J. Whitmer, K. Hoffmann, M. Tirrell and J. J. de Pablo, *ACS Macro Lett.*, 2014, **3**, 565–568.

11 K. A. Black, D. Priftis, S. L. Perry, J. Yip, W. Y. Byun and M. Tirrell, *ACS Macro Lett.*, 2014, **3**, 1088–1091.

12 S. Gao, A. Holkar and S. Srivastava, *Polymers*, 2019, **11**, 1097.

13 A. F. Mason, B. C. Buddingh, D. S. Williams and J. C. M. Van Hest, *J. Am. Chem. Soc.*, 2017, **139**, 17309–17312.

14 N. Martin, M. Li and S. Mann, *Langmuir*, 2016, **32**, 5881–5889.

15 A. C. Obermeyer, C. E. Mills, X. H. Dong, R. J. Flores and B. D. Olsen, *Soft Matter*, 2016, **12**, 3570–3581.

16 A. Nolles, A. H. Westphal, J. A. De Hoop, R. G. Fokkink, J. M. Kleijn, W. J. H. Van Berkel and J. W. Borst, *Biomacromolecules*, 2015, **16**, 1542–1549.

17 E. Sokolova, E. Spruijt, M. M. K. Hansen, E. Dubuc, J. Groen, V. Chokkalingam, A. Piruska, H. A. Heus and W. T. S. Huck, *Proc. Natl. Acad. Sci. U. S. A.*, 2013, **110**, 11692–11697.

18 T. Z. Jia, *Doctoral Dissertation*, Harvard University, 2016.

19 R. R. Poudyal, C. D. Keating and P. C. Bevilacqua, *ACS Chem. Biol.*, 2019, **14**, 1243–1248.

20 A. A. M. André and E. Spruijt, *Biophys. J.*, 2018, **115**, 1837–1839.

21 J. R. Vieregg and T. Y. D. Tang, *Curr. Opin. Colloid Interface Sci.*, 2016, **26**, 50–57.

22 D. Priftis, L. Leon, Z. Song, S. L. Perry, K. O. Margossian, A. Tropnikova, J. Cheng and M. Tirrell, *Angew. Chem., Int. Ed.*, 2015, **54**, 11128–11132.

23 S. Koga, D. S. Williams, A. W. Perriman and S. Mann, *Nat. Chem.*, 2011, **3**, 720–724.

24 E. Duhoranimana, E. Karangwa, L. Lai, X. Xu, J. Yu, S. Xia, X. Zhang, B. Muhoza and I. Habinshuti, *Food Hydrocolloids*, 2017, **69**, 111–120.

25 R. J. Ellis, *Trends Biochem. Sci.*, 2001, **26**, 597–604.

26 B. van den Berg, R. Wain, C. M. Dobson and R. J. Ellis, *EMBO J.*, 2000, **19**, 3870–3875.

27 A. P. Minton, *Curr. Biol.*, 2006, **16**, 269–271.

28 A. P. Minton, *J. Biol. Chem.*, 2001, **276**, 10577–10580.

29 A. P. Minton, *J. Pharm. Sci.*, 2005, **94**, 1668–1675.

30 T. Kojima and S. Takayama, *ACS Appl. Mater. Interfaces*, 2018, **10**, 32782–32791.

31 R. Toor, L. Hourdin, S. Shanmugathasan, P. Lefrançois, S. Arbault, V. Lapeyre, L. Bouffier, J. Douliez, V. Ravaine and A. Perro, *J. Colloid Interface Sci.*, 2023, **629**, 46–54.

32 D. E. Discher and A. Eisenberg, *Science*, 2002, **297**, 967–973.

33 E. Rideau, R. Dimova, P. Schwille, F. R. Wurm and K. Landfester, *Chem. Soc. Rev.*, 2018, **47**, 8572–8610.

34 X. Wang, S. Moreno, S. Boye, P. Wang, X. Liu, A. Lederer, B. Voit and D. Appelhans, *Adv. Sci.*, 2021, **8**, 1–13.

35 F. Zhao, G. Shen, C. Chen, R. Xing, Q. Zou, G. Ma and X. Yan, *Chem. – A Eur. J.*, 2014, **20**, 6880–6887.

36 P.-A. Monnard and D. W. Deamer, *Origins Life Evol. Biospheres*, 2001, **31**, 147–155.

37 P. M. McCall, S. Srivastava, S. L. Perry, D. R. Kovar, M. L. Gardel and M. V. Tirrell, *Biophys. J.*, 2018, **114**, 1636–1645.

38 A. Oparin, *Orig. Life*, 1976, **7**, 3–8.

39 *Protocells*, ed. S. Rasmussen, M. A. Bedau, L. Chen, D. Deamer, D. C. Krakauer, N. H. Packard and P. F. Stadler, The MIT Press, 2008.

40 S. Liu, Y. Zhang, M. Li, L. Xiong, Z. Zhang, X. Yang, X. He, K. Wang, J. Liu and S. Mann, *Nat. Chem.*, 2020, **12**, 1165–1173.

41 S. Barthold, S. Kletting, J. Taffner, C. de Souza Carvalho-Wodarz, E. Lepeltier, B. Loretz and C.-M. Lehr, *J. Mater. Chem. B*, 2016, **4**, 2377–2386.

42 J. K. Bediako, J. H. Kang, Y. S. Yun and S. H. Choi, *ACS Appl. Polym. Mater.*, 2022, **4**, 2346–2354.

43 W. Zhao, Y. Fan, H. Wang and Y. Wang, *Langmuir*, 2017, **33**, 6846–6856.

44 D. J. Iyer, A. Holkar and S. Srivastava, *Advances in Water Desalination Technologies*, World Scientific, 2020, vol. 17, pp. 129–167.

45 B. Liu, Y. Fan, H. Li, W. Zhao, S. Luo, H. Wang, B. Guan, Q. Li, J. Yue, Z. Dong, Y. Wang and L. Jiang, *Adv. Funct. Mater.*, 2021, **31**, 1–11.

46 L. Zhang, J. Wang, Y. Fan and Y. Wang, *Adv. Sci.*, 2023, **10**, 1–12.

47 Z. Xiao, W. Liu, G. Zhu, R. Zhou and Y. Niu, *J. Sci. Food Agric.*, 2014, **94**, 1482–1494.

48 S. Leclercq, K. R. Harlander and G. A. Reineccius, *Flavour Fragr. J.*, 2009, **24**, 17–24.

49 Y. P. Timilsena, T. O. Akanbi, N. Khalid, B. Adhikari and C. J. Barrow, *Int. J. Biol. Macromol.*, 2019, **121**, 1276–1286.

50 C. Fick, Z. Khan and S. Srivastava, *Mater. Adv.*, 2023, **4**, 4665–4678.

51 F. Pir Cakmak, A. T. Grigas and C. D. Keating, *Langmuir*, 2019, **35**, 7830–7840.

52 A. D. Dinsmore, M. F. Hsu, M. G. Nikolaides, M. Marquez, A. R. Bausch and D. A. Weitz, *Science*, 2002, **298**, 1006–1009.

53 M. Li, X. Huang, T. Y. D. Tang and S. Mann, *Curr. Opin. Chem. Biol.*, 2014, **22**, 1–11.

54 J. Li, X. Liu, L. K. E. A. Abdelmohsen, D. S. Williams and X. Huang, *Small*, 2019, **15**, 1902893.

55 A. W. Folkmann, A. Putnam, C. F. Lee and G. Seydoux, *Science*, 2021, **373**, 1218–1224.

56 W. J. Altenburg, N. A. Yewdall, D. F. M. Vervoort, M. H. M. E. van Stevendaal, A. F. Mason and J. C. M. van Hest, *Nat. Commun.*, 2020, **11**, 6282.

57 D. van Swaay, T.-Y. D. Tang, S. Mann and A. de Mello, *Angew. Chem.*, 2015, **127**, 8518–8521.

58 N. N. Deng and W. T. S. Huck, *Angew. Chem., Int. Ed.*, 2017, **56**, 9736–9740.

59 T. Beneyton, C. Love, M. Girault, T.-Y. D. Tang and J. Baret, *ChemSystemsChem*, 2020, **2**, e2000022.

60 H. Seo and H. Lee, *Nat. Commun.*, 2022, **13**, 5179.

61 C. E. Sing, *Adv. Colloid Interface Sci.*, 2017, **239**, 2–16.

62 S. L. Perry, *Curr. Opin. Colloid Interface Sci.*, 2019, **39**, 86–97.

63 A. M. Rumyantsev, N. E. Jackson and J. J. de Pablo, *Annu. Rev. Condens. Matter Phys.*, 2021, **12**, 155–176.

64 L. Chang, T. K. Lytle, M. Radhakrishna, J. J. Madinya, J. Vélez, C. E. Sing and S. L. Perry, *Nat. Commun.*, 2017, **8**, 1273.

65 J. R. Magana, C. C. M. Sproncken and I. K. Voets, *Polymers*, 2020, **12**, 1953.

66 S. Srivastava, M. Andreev, A. E. Levi, D. J. Goldfeld, J. Mao, W. T. Heller, V. M. Prabhu, J. J. de Pablo and M. V. Tirrell, *Nat. Commun.*, 2017, **8**, 14131.

67 D. Iyer, V. M. S. Syed and S. Srivastava, *J. Polym. Sci.*, 2021, **59**, 2895–2904.

68 L. Li, S. Srivastava, M. Andreev, A. B. Marciel, J. J. de Pablo and M. V. Tirrell, *Macromolecules*, 2018, **51**, 2988–2995.

69 D. Priftis, N. Laugel and M. Tirrell, *Langmuir*, 2012, **28**, 15947–15957.

70 J. Fu, R. L. Abbett, H. M. Fares and J. B. Schlenoff, *ACS Macro Lett.*, 2017, **6**, 1114–1118.

71 P. Schaaf and J. B. Schlenoff, *Adv. Mater.*, 2015, **27**, 2420–2432.

72 Z. A. Digby, M. Yang, S. Lteif and J. B. Schlenoff, *Macromolecules*, 2022, **55**, 978–988.

73 V. M. S. Syed and S. Srivastava, *ACS Macro Lett.*, 2020, **9**, 1067–1073.

74 A. B. Marciel, S. Srivastava and M. V. Tirrell, *Soft Matter*, 2018, **14**, 2454–2464.

75 D. F. Parsons, M. Boström, P. Lo Nostro and B. W. Ninham, *Phys. Chem. Chem. Phys.*, 2011, **13**, 12352.

76 K. W. Mattison, I. J. Brittain and P. L. Dubin, *Biotechnol. Prog.*, 1995, **11**, 632–637.

77 C. L. Cooper, P. L. Dubin, A. B. Kayitmazer and S. Turksen, *Curr. Opin. Colloid Interface Sci.*, 2005, **10**, 52–78.

78 H. C. Van de Hulst and V. Twersky, *Phys. Today*, 1957, **10**, 28–30.

79 C. Mätzler, *IAP Res. Rep.*, 2002, 1139–1151.

80 S. R. Reddy and H. S. Fogler, *J. Colloid Interface Sci.*, 1981, **79**, 101–104.

81 H. Wang and R. H. Davis, *J. Colloid Interface Sci.*, 1993, **159**, 108–118.

82 S. K. Friedlander and W. H. Marlow, *Phys. Today*, 1977, **30**, 58–59.

83 A. E. Neitzel, Y. N. Fang, B. Yu, A. M. Rumyantsev, J. J. De Pablo and M. V. Tirrell, *Macromolecules*, 2021, **54**, 6878–6890.

84 T. K. Lytle, L. W. Chang, N. Markiewicz, S. L. Perry and C. E. Sing, *ACS Cent. Sci.*, 2019, **5**, 709–718.

85 S. Kim, M. Lee, W. B. Lee and S. H. Choi, *Macromolecules*, 2021, **54**, 7572–7581.

86 J. Esquena, *Curr. Opin. Colloid Interface Sci.*, 2016, **25**, 109–119.